Supplement of Atmos. Chem. Phys., 23, 389–415, 2023
https://doi.org/10.5194/acp-23-389-2023-supplement

Atmospheric Chemistry and Physics
Open Access
EGU

Supplement of

A full year of aerosol size distribution data from the central Arctic under an extreme positive Arctic Oscillation: insights from the Multidisciplinary drifting Observatory for the Study of Arctic Climate (MOSAiC) expedition

Matthew Boyer et al.

Correspondence to: Matthew Boyer (matthew.boyer@helsinki.fi) and Julia Schmale (julia.schmale@epfl.ch)

Pollution masking

An important considering when using the ARM aerosol data from the MOSAiC is the inlet purge blower in the AOS container. An inlet purge blower designed specifically for this campaign was installed on the AOS inlet. The purge blower was set to deliver a continuous flow of particle-free air into the inlet of the AOS during times when pollution was detected, effectively purging the inlet with clean air. Pollution detection was carried out according to elevated carbon monoxide (CO) mixing ratios from a sample line collocated with the AOS inlet; above a given CO threshold, the purge blower was triggered. There were issues with the automated triggering system because of low CO emissions from the ship stack during this campaign. In general, CO is not an ideal indicator for ship pollution (Celik et al., 2020). Instead, the purge blower was manually turned on when pollution was apparent in the aerosol data for extended periods. The purge blower was developed to detect and protect the instruments from contamination during pollution events, however, the data collected during times when the purge blower was enabled is not representative of ambient aerosol and was removed from the aerosol size distribution data used in this study. Due to the improper operation of the automated purge blower, there were still times when the AOS inlet was sampling local pollution, and hence the use of the pollution detection algorithm as described in the main text (Section 2.4).

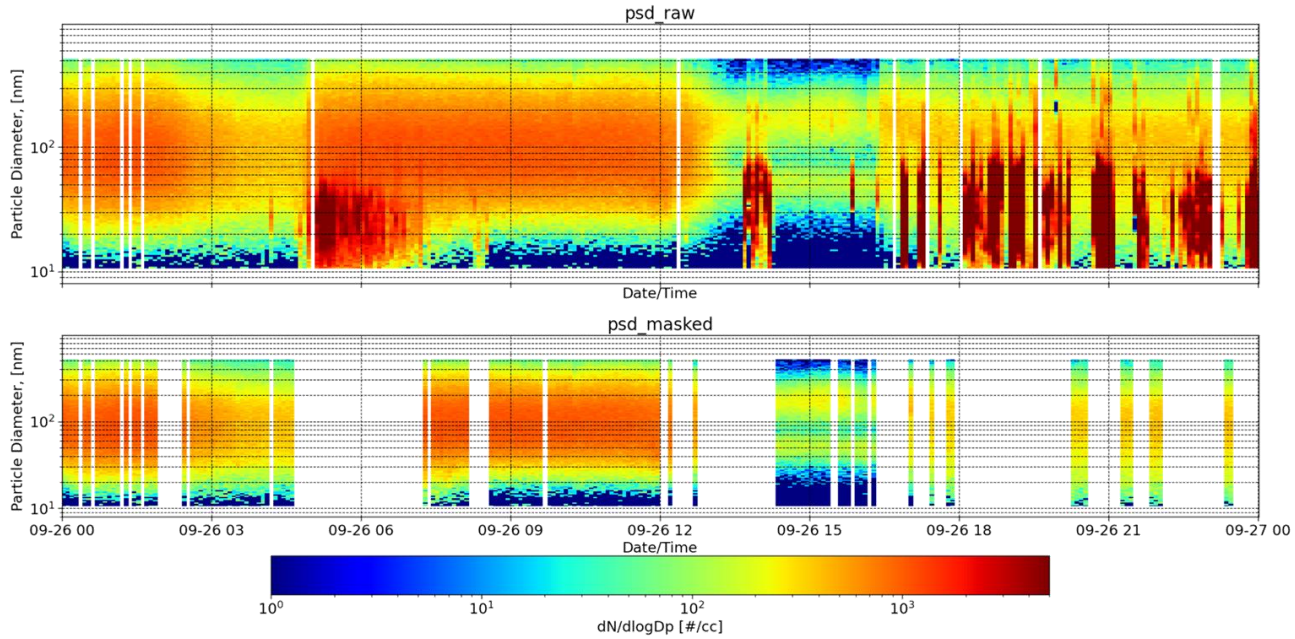

Fig. S1. A comparison of the aerosol size distribution data before and after applying the pollution detection algorithm to remove local pollution. This figure shows a single day of aerosol size distribution data on September 26, 2020 as an example to show the performance of the pollution removal method (see methods). The pollution detection algorithm, developed by Beck et al. (2022), was applied to raw aerosol size distribution data (top) to produce a data set with the influence of local pollution sources removed (bottom). Note that pollution from the ship was typically characterized by very high concentrations of particles lower than ~70 nm. The concurrent appearance of the enhanced accumulation mode with the pollution signal in the PNSD at ~ 05:00 during this example is coincidental.

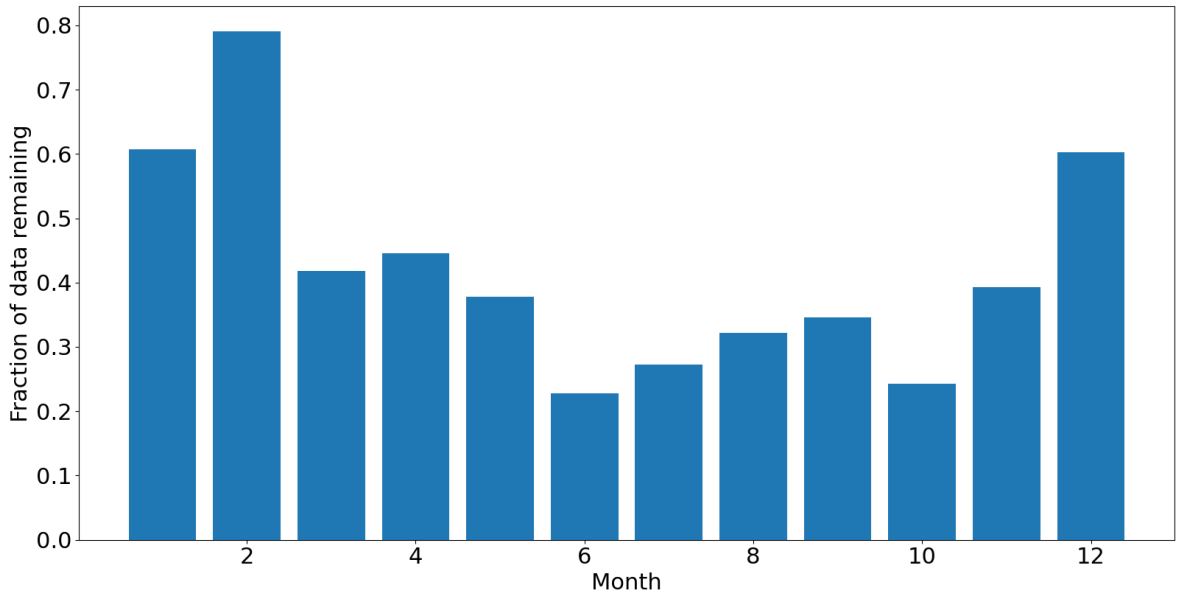

Fig. S2. The fraction of the aerosol size distribution data remaining, per month, after applying the pollution detection algorithm. Note that 42% of the annual aerosol size distribution dataset remained after application of the pollution detection algorithm.

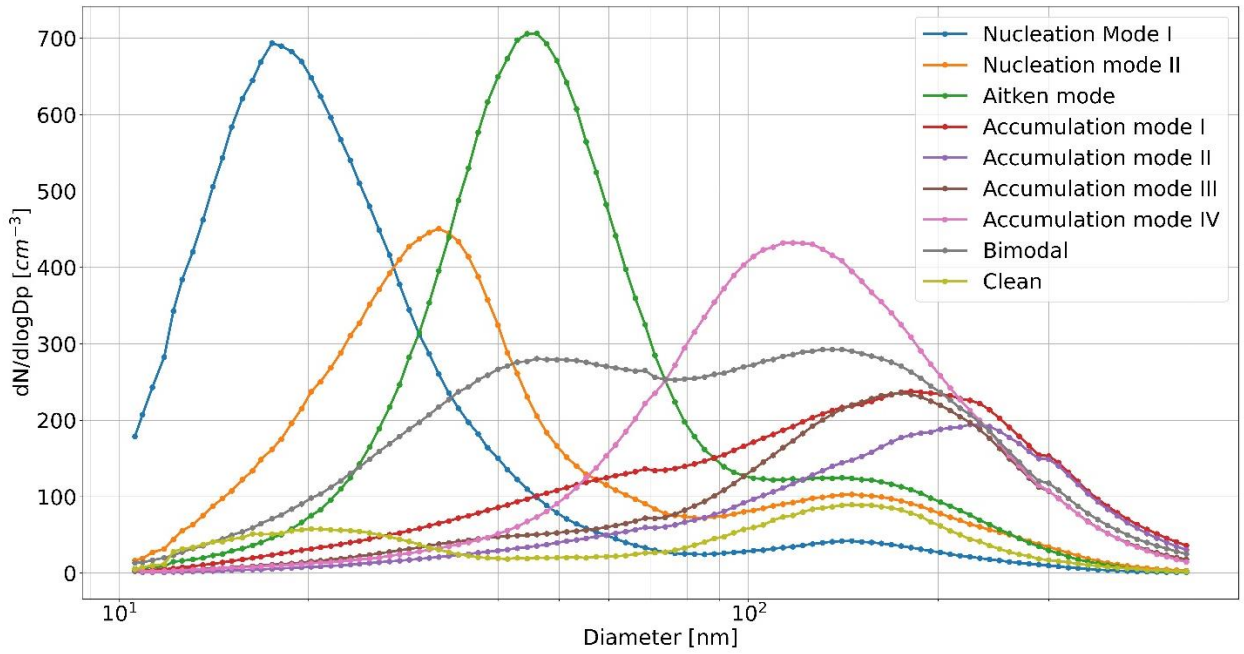

Fig. S3. The average distributions of the nine PNSD clusters. The particle concentration in units of $dN/dlogD_p$ is presented for the daily average of each of the nine original clusters according to the particle size. In Fig. 3 in the main text, the four accumulation mode clusters were manually grouped into a single accumulation mode cluster, and the two nucleation mode clusters were combined into a single nucleation mode cluster to simplify interpretation.

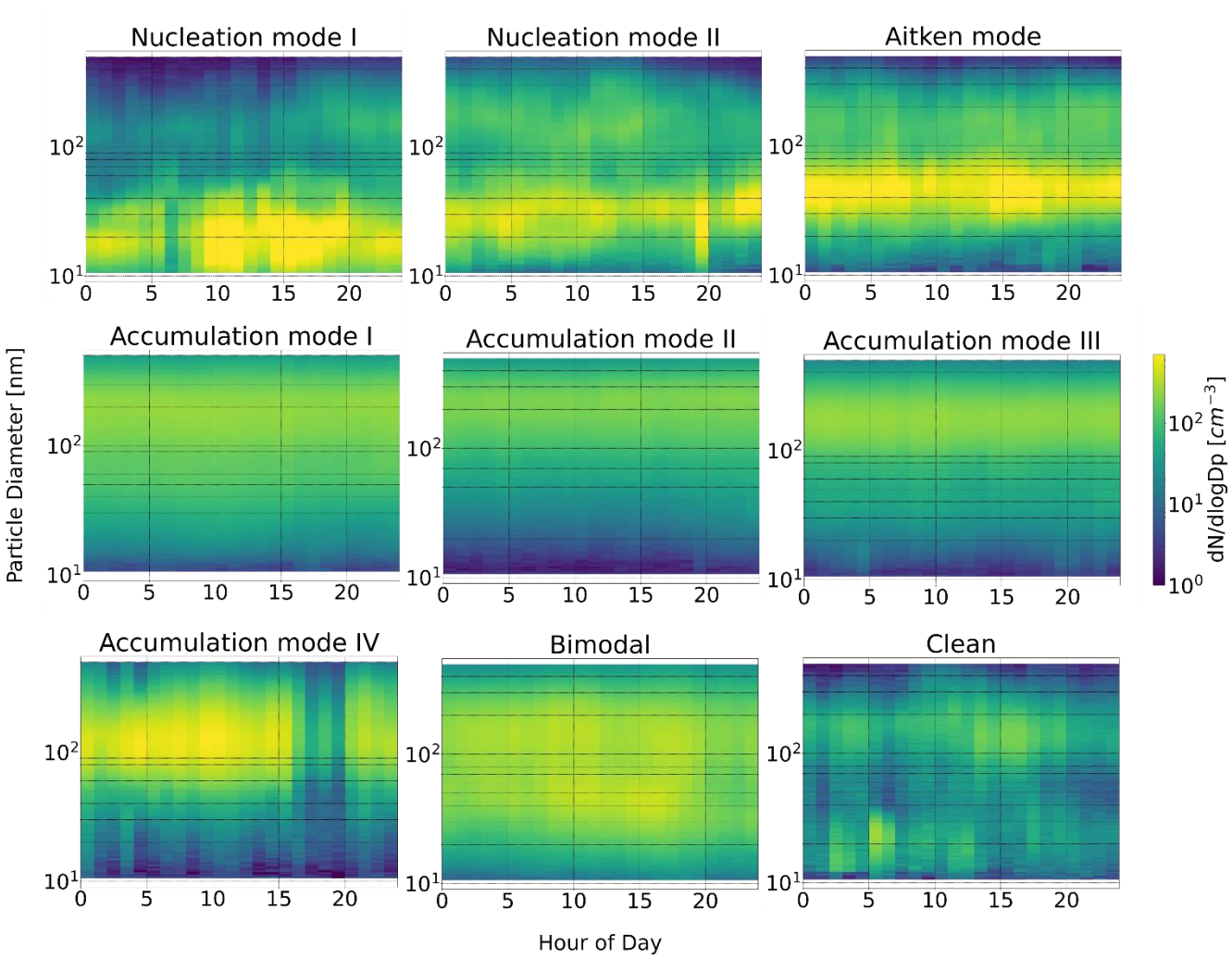

Fig. S4. The disaggregated daily PNSD clusters. Each surface plot shows the hourly aggregated averages of the PNSD for each day that is described by the given clusters. The color bar depicts the particle concentration in units of $dN/dlogD_p$. Beddows et al., (2014) proposed this approach to present the diurnal cycle associated with each daily cluster type. While the diurnal cycles for the clusters are not meaningful in this data due to polar day/night and inconsistencies in the timing of pollution, these figures show addition details into the variation of each daily cluster type.

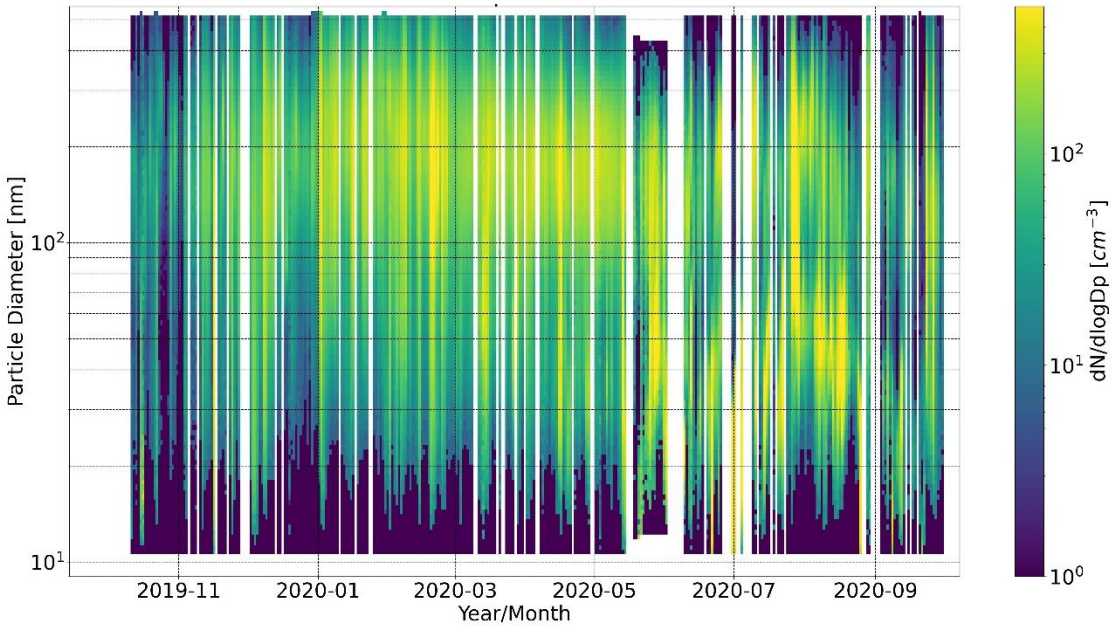

Fig. S5. The annual cycle of the PNSD during MOSAiC presented as daily medians.

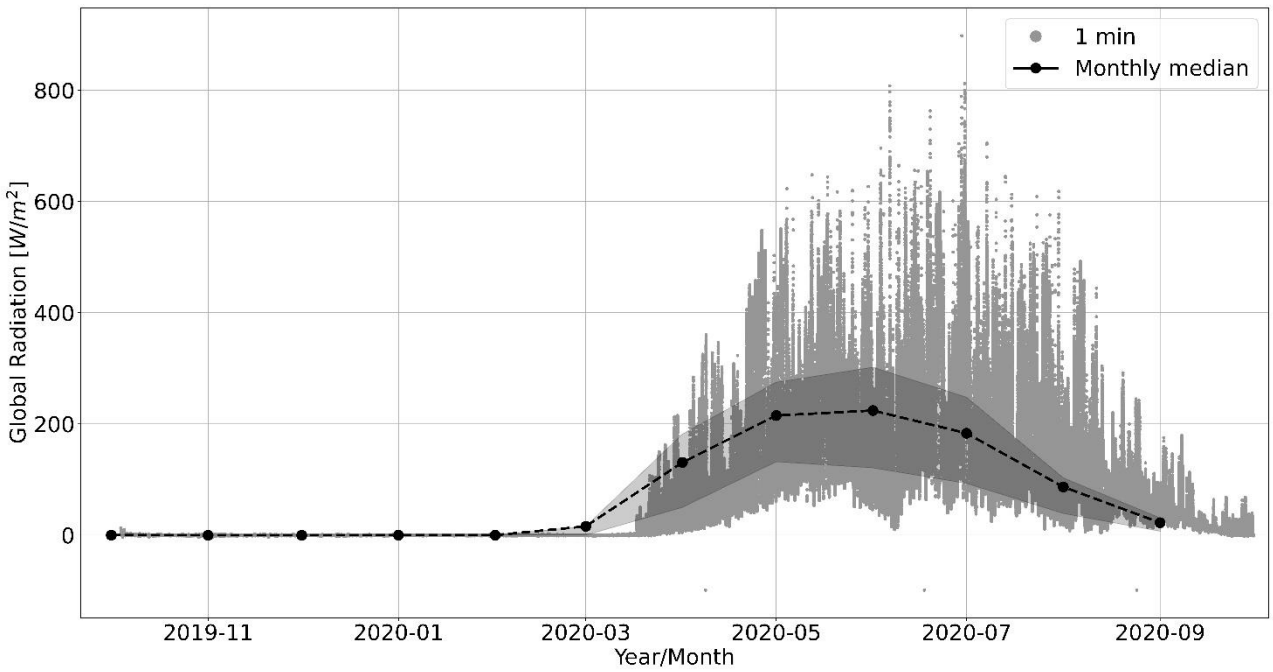

Fig. S6. The annual cycle of global radiation on *Polarstern*. The dotted line presents the data as the monthly medians and the shaded region shows the interquartile range.

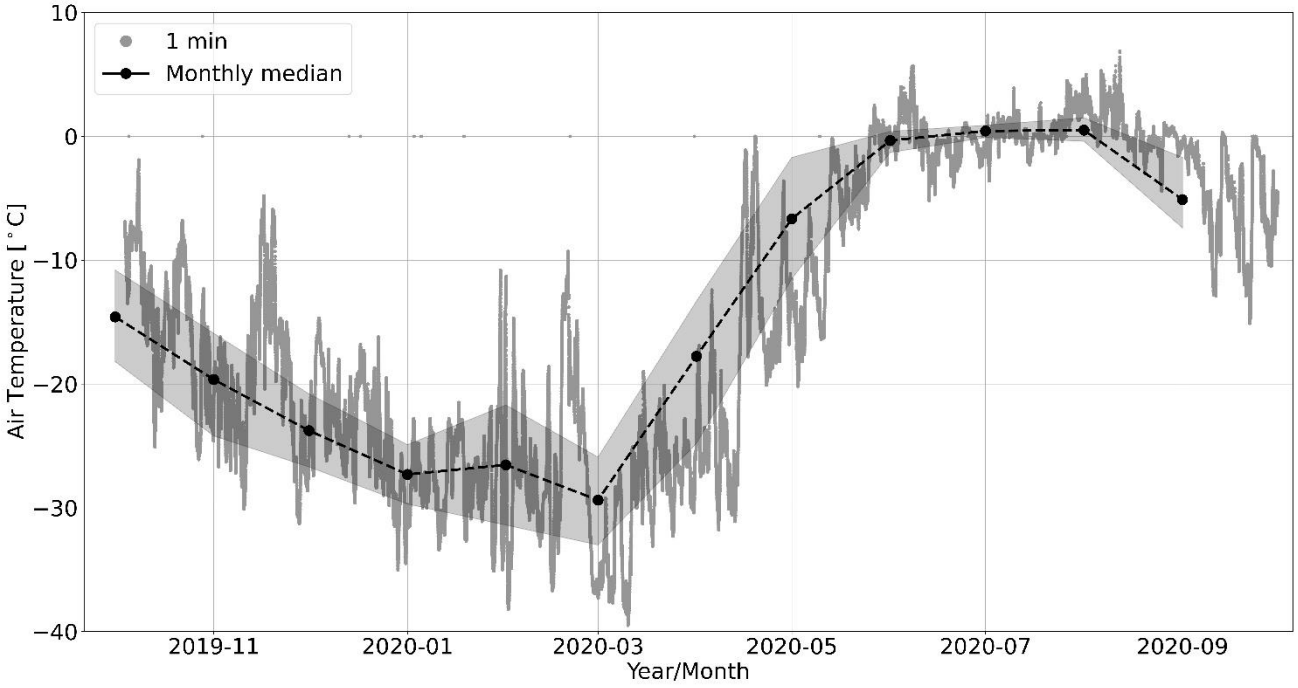

Fig. S7. The annual cycle of air temperature on *Polarstern*. The dotted line presents the data as the monthly median and the shaded region shows interquartile range.

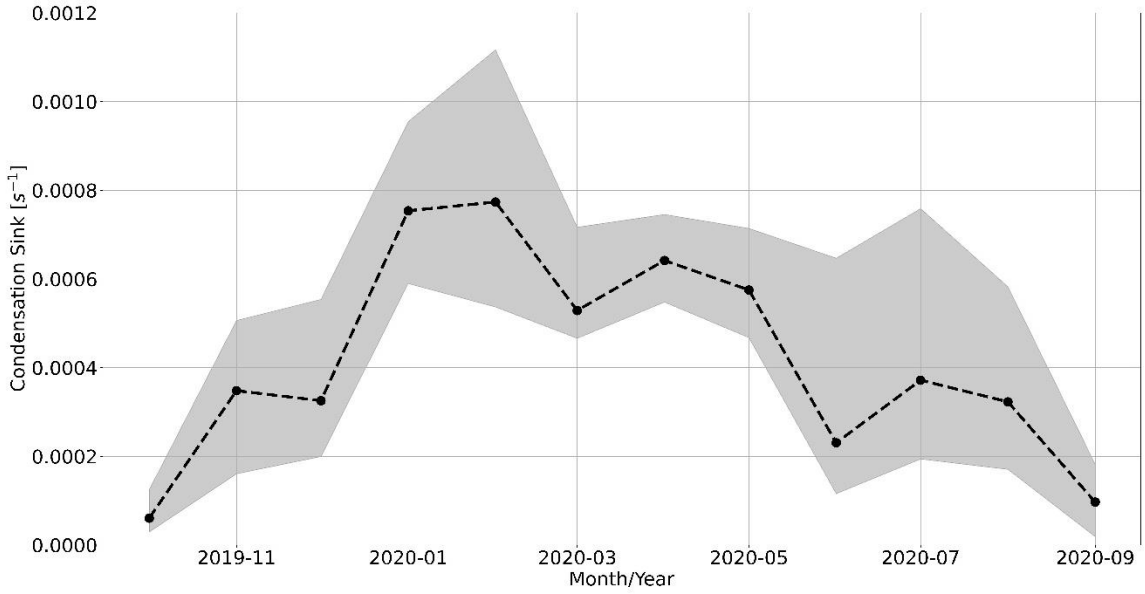

Fig. S8. The annual cycle in the condensation sink. The condensation sink represents the loss of condensable vapors onto pre-existing aerosol surfaces. The shaded region shows the interquartile range.

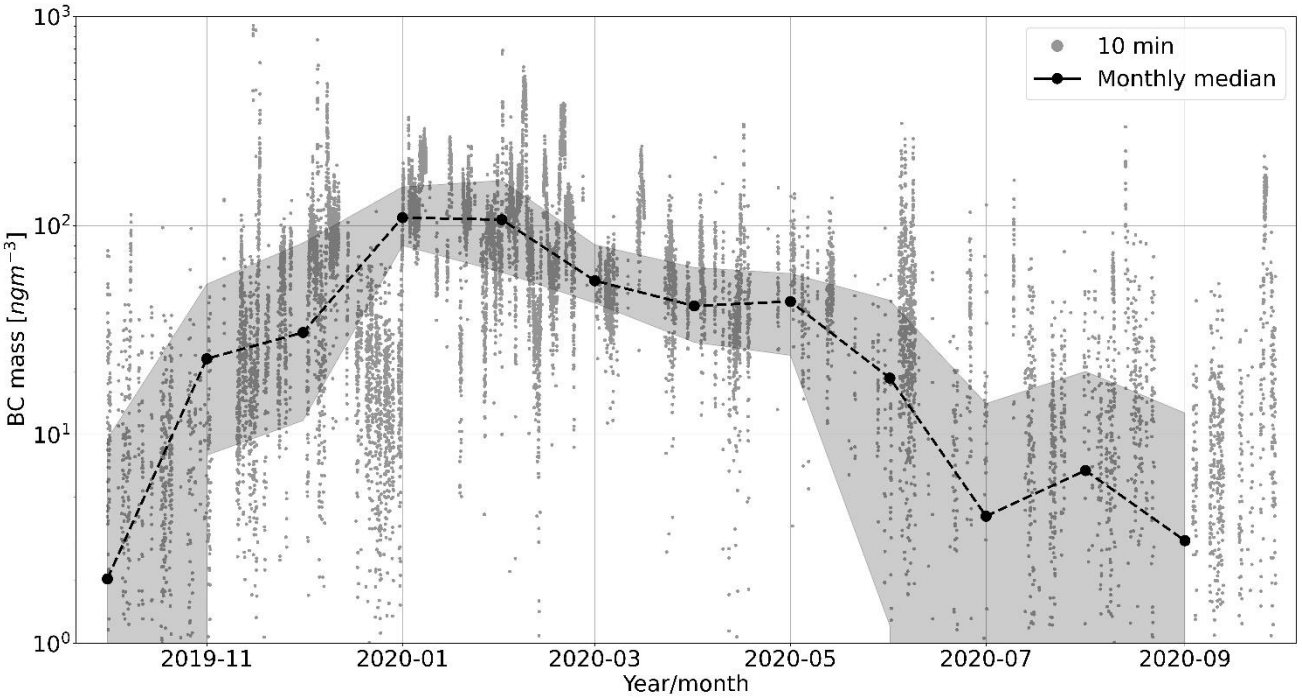

Fig. S9. The annual cycle of the BC mass concentrations during MOSAiC. The data is presented at time resolution of 10 min with the monthly median concentrations overlayed for context. The shaded region shows the interquarile range.

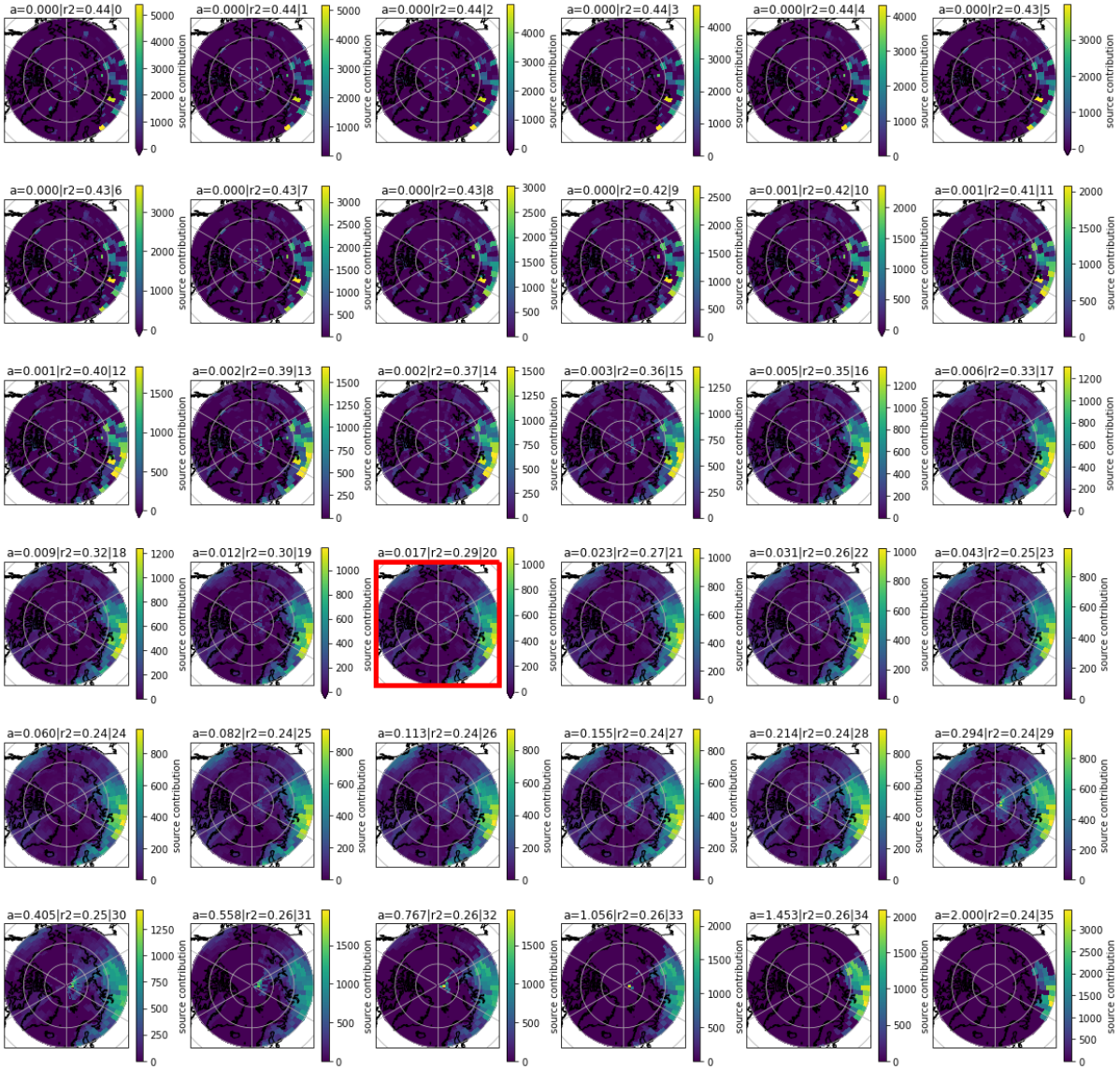

Fig. S10. The 36 source region footprint maps of BC produced using the iterative elastic net regularization method in the inverse model. The polygons represent the source region locations identified by the inverse model for various levels of penalization of the hyperparameters in the elastic net regression method. Iteration 20, outlined in red, was selected for further analysis of BC as it represents known source regions while minimizing the influence from noise.

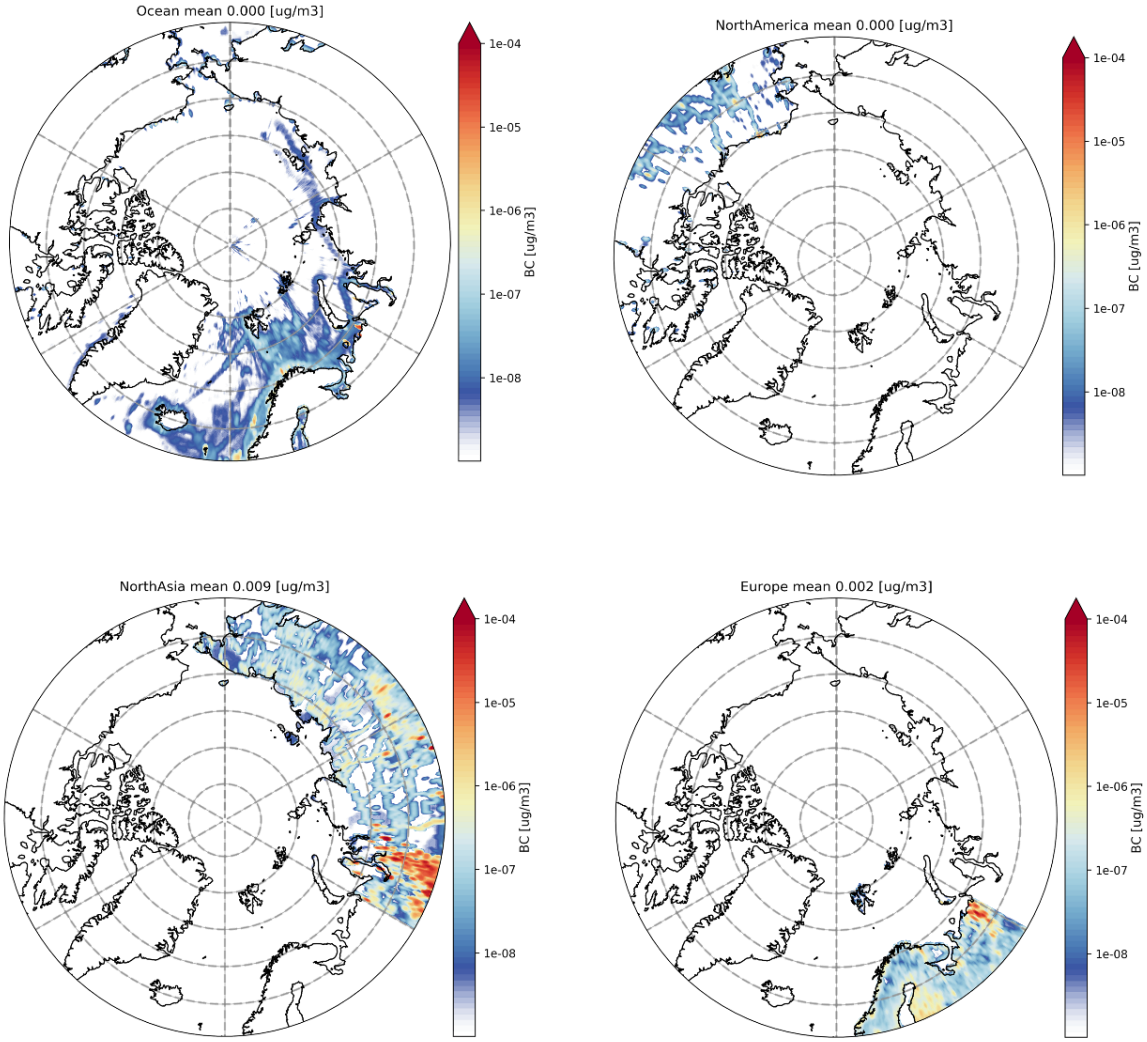

Fig. S11. Annual mean source contribution maps of BC from the ECLIPSE v6b emission inventory coupled with the seasonal FES. The sources regions are divided using the same geographic mask as Figure 2.

References

Celik, S., Drewnick, F., Fachinger, F., Brooks, J., Darbyshire, E., Coe, H., Paris, J.-D., Eger, P. G., Schuladen, J., Tadic, I., Friedrich, N., Dienhart, D., Hottmann, B., Fischer, H., Crowley, J. N., Harder, H., and Borrmann, S.: Influence of vessel characteristics and atmospheric processes on the gas and particle phase of ship emission plumes: in situ measurements in the Mediterranean Sea and around the Arabian Peninsula, Atmos. Chem. Phys., 20, 4713–4734, https://doi.org/10.5194/acp-20-4713-2020, 2020.